Effect of Uniaxial Stretching on the Tensile Impact Test for Poly(ethylene Terephthalate)

MITSURU YOKOUCHI, YASUYUKI HIROMOTO, and YASUJI KOBAYASHI, *Department of Industrial Chemistry, Faculty of Technology, Tokyo Metropolitan University, Fukazawa, Setagaya-ku, Tokyo 158, Japan*

Synopsis

In order to correlate impact strength with the structure of polymeric materials, a tensile impact test was carried out using a uniaxially stretched poly(ethylene terephthalate) (PET) sheet. The structural factors were the draw ratio (λ) and the cut-out angle (θ) under the conditions of constant impacting speed (10.5 m/sec = 1.8×10^4%/sec) and temperature (20° ± 1°C). The occurrence of structural anisotropy by stretching of isotropic amorphous quench-rolled PET was classified into three drawing stages: $\lambda = -1.5$ or 2.0, -3.5, and over 3.5. This is related to a deformation mechanism of masses with dimensions a few tenths of a μm and their boundaries. The boundaries are not clear until adiabatic deformation (mechanical impact) is applied. The area supporting the mechanical strength was limited to just a small section. Its character was affected by macroscopic deformation only in the direction parallel or near to the stretching direction, since the mechanical properties were not changed for the range of the cut-out angle θ = 45–90°.

INTRODUCTION

Since polymeric substances are utilized for structural parts, studies of mechanical properties and tests under impacting speeds are performed to simulate those encountered in practice. However, results of various standard tests do not correlate with one another, since the data obtained depend on the preparation conditions of the test pieces and many other factors in the measurement process.

In this study, tensile impact testing was performed for uniaxially stretched polymer sheets (width unrestrained) as a simple system design. One purpose of the study was to elucidate to what extent the factors control the characteristics of impact breaking of polymeric materials. It may be said that a sheet satisfies the requirement for uniformity as a starting material for many test specimens. The apparent structural factors are only the draw ratio and the cut-out angle, under the conditions of constant testing speed and temperature. Generally, structural anisotropy occurs by uniaxial orientation. If the variation of impact characteristics is clarified, this study can provide additional information for changes of molecular structure and morphology by stretching. The adoption of the tensile impact test is based on the premise that, since a stress–strain curve can be observed in a very short time (several msec), the effect of relaxation of macromolecules is not so significant. The results reflect the internal structure of the test specimens (e.g., state of orientation).

Journal of Applied Polymer Science, Vol. 24, 1965–1975 (1979)

0021-8995/79/0024-1965$01.00

EXPERIMENTAL

Specimens

Undrawn and quench-rolled poly(ethylene terephthalate) (PET), $[—OCH_2CH_2O—CO\phi CO—]_n$, sheet, supplied by Teijin Co. Ltd., was used as a starting material throughout this study (260 μm thick and density 1.344 g/cm^3). This sheet was found to be isotropic, with no orientation observed by an optical microscope. In order to obtain samples of different orientation, the sheets were placed in an air oven at 80°C for 12 min and drawn uniaxially at a rate of 30%/min to various lengths, followed by cooling to room temperature. Specimens for tensile impact testing (5 × 90 mm) were prepared from the above elongated sheets. The cut-out angle ranged from parallel to perpendicular (at intervals of 15°) to the stretched direction. Both end parts of the specimens were reinforced by an adhesive tape made of aluminum foil. The lengths corresponded with those of the halved Morse-type taper pins (11 and 21 mm, respectively) of the rear and front specimen clamps of the tensile impact apparatus. The specimen dimensions for tensile impact testing were 5 × 58 mm (Fig. 1).

Tensile Impact Testing

A flywheel-type tensile impact tester with a new load cell was designed and fabricated for specimens of polymer sheet and film. This apparatus employed a piezoelectric ceramic oscillator (toric in shape) as a load sensor. It has a high natural frequency (1800 kHz) and sensitivity (ca. 0.1 V/N). Signals of impact were recorded by a transient time converter (Riken Denshi). This was equipped with a memorization system (5 μsec at maximum resolution), an automatic pretrigger circuit, and a facility for reproduction under a slower time base, thus eliminating the need for troublesome photography. Details of the characteristics and operating procedures of this apparatus have been reported previously.[1,2]

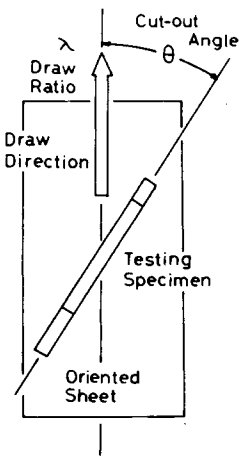

Fig. 1. Preparation of a specimen for tensile impact testing with draw ratio λ and cut-out angle θ.

Density

Density of the samples were measured at 20°C in a density gradient column composed of n-heptane and carbon tetrachloride. After soaking in the column, the position of the specimen was read at intervals of 1, 2, 4, 8, and 16 min and then plotted against the reciprocal of the root of the measurement time. The observed density was estimated by extrapolation of the curve to infinite time.

Birefringence

Birefringence measurements of the samples were carried out with α-bromonaphthalene and methylene diiodide, using an Abbé refractometer at room temperature. The values were defined as the differences in refractive indices parallel and perpendicular to the draw direction.

SEM Observation

Breaking surfaces of specimens after impact testing were observed by using scanning electron microscopy. The samples were coated with a thin layer (ca. 10 nm thick) of gold to prevent charging with electricity.

RESULTS AND DISCUSSION

Dependence on Impact Speed

From the stress–strain curve during impact (Fig. 2), the following values were calculated: (1) modulus of elasticity E, (2) tensile stress at yield σ_y, (3) tensile stress at breaking σ_b, (4) true strain until failure ϵ_b, and (5) breaking energy indicated by area under the stress–strain curve S_b. The values of σ_b, after yielding followed by plastic deformation (which may be very high due to orientation hardening) do not accurately reflect the physical properties of the test specimens. Moreover, they are difficult to calculate since the cross section changed significantly. Instead of σ_y and σ_b, maximum stress (σ_m) was considered, which corresponds to σ_y when the yield is observed and to σ_b when rupture occurs at the initial deformation stage.

Using the appointed shape of the test specimen of the undrawn PET sheet, the dependence of each mechanical property described above on impacting speed (from 100 rpm = 2.6 m/sec = 4.5×10^3%/sec to 900 rpm = 23.6 m/sec = 4.1×10^4%/sec) was examined. The obtained stress–strain curves all indicated brittle fracture. The values of E, σ_m, ϵ_b, and S_b increased slightly and gradually with augmentation of the flywheel revolution speed, and became maximum at 700 rpm. The effect of impacting speed in the present study was insignificant. For example, the variation of σ_m is shown in Figure 3. However, in the range of 800–900 rpm, the dispersion altered dramatically, having extremely high values. This indicated a structural change in the fracture mechanism. The structural defects (voids and cracks) in the specimen, rather than the molecular and fine structure, play a great role in the mechanical properties.

Therefore, the impacting speed was fixed at 400 rpm = 10.5 m/sec = 1.8×10^4%/sec for specimens with varying degrees of uniaxial orientation, where the dispersion was relatively minor.

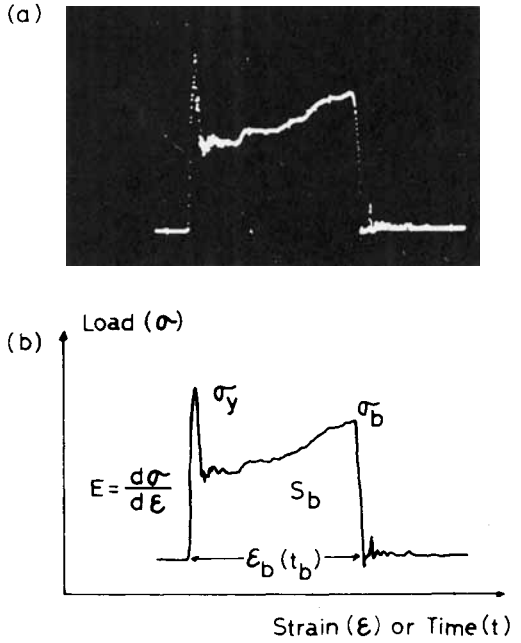

Fig. 2. (a) Photograph of a typical load–time impact curve of PET sheet with resolution of 25 μsec on the cathode ray tube of a transient time converter (400 rpm = 10.5 m/sec = 1.8×10^4%/sec at 20°C). (b) Recorded curve (a) and definition of the five mechanical properties: initial Young's modulus E, load at yielding σ_y, breaking load σ_b, breaking strain ϵ_b, and breaking energy S_b.

Dependence on Draw Ratio and Cut-Out Angle

When the test specimens varied with respect to draw ratio and cut-out angle, the mechanical properties were affected. The method for plotting the observed data is described below. The mechanical properties (E, σ_m, ϵ_b, and S_b) were plotted against the polar coordinates (λ, θ), where λ is the draw ratio and θ is the cut-out angle to the elongated direction. The state of the test specimen is explicitly represented by the polar coordinates (λ, θ). The results are shown for the initial Young's modulus, the maximum load, the breaking strain, and the breaking energy in Figures 4–7, respectively. It was found that E and σ_m and

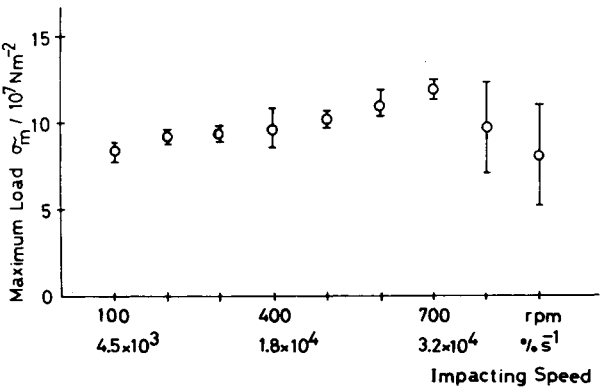

Fig. 3. Dependence of maximum load on impacting speed at 20° ± 1°C for amorphous quench-rolled PET sheet.

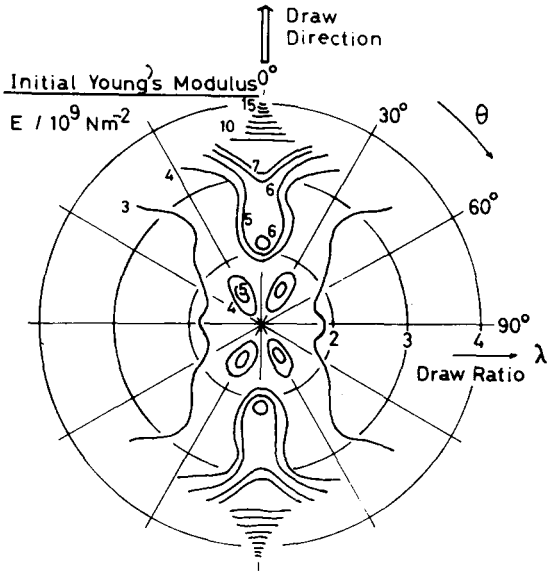

Fig. 4. Dependence of Young's modulus E on draw ratio λ and cut-out angle θ for PET sheet at impacting speed of 10.5 m/sec = 1.8×10^4%/sec at 20° ± 1°C.

ϵ_b and S_b show similar patterns, respectively. In the case of the former parameters when $\lambda = 1.5$–2.0, the drawn polymer is in the "preorientation state," [9] and the maximum E or σ_m is observed in the direction of approximately $\theta = 30°$. For a larger draw ratio the increase becomes pronounced, being restricted to a narrower cut-out angle against the draw direction; and above $\lambda = 3.5$ the tendency becomes very remarkable. For parameters ϵ_b and S_b when $\lambda = 1.5$–2.0, brittle fracture occurs, and further elongation gives rise to ductile fracture; but at $\lambda >$

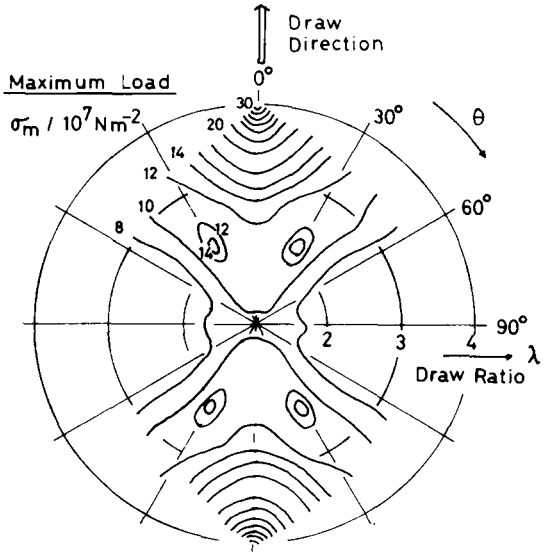

Fig. 5. Dependence of maximum load σ_m on draw ratio λ and cut-out angle (θ) for PET sheet at impacting speed of 10.5 m/sec = 1.8×10^4%/sec at 20° ± 1°C.

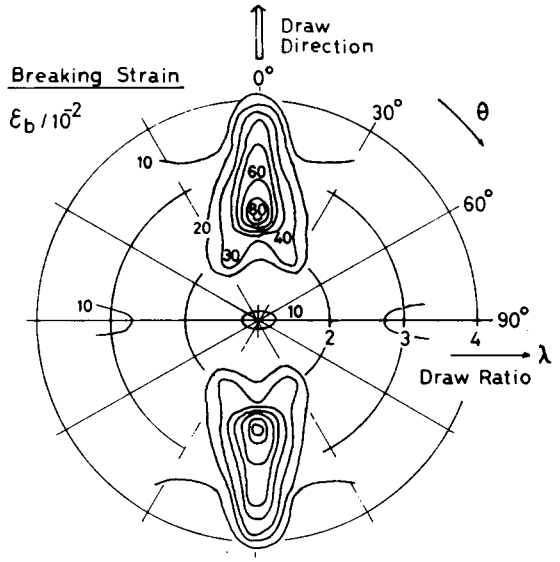

Fig. 6. Dependence of breaking strain ϵ_b on draw ratio λ and cut-out angle θ for PET sheet at impacting speed of 10.5 m/sec = 1.8×10^4%/sec at 20° ± 1°C.

3.5 the polymer is no longer ductile, and again the features of brittleness begin to appear. Also all the above figures indicate that in the range of a cut-out angle θ = 45–90°, addition or reduction of the values of E, σ_m, ϵ_b, and S_b does not occur. These figures can be compared with those of the unoriented starting material, even when the draw ratio is varied. Although the orientational behavior appears to be monotoic, the occurrence of mechanical anisotropy by elongation is not simple. Mechanical anisotropy can be classified into the following three stages: $\lambda = -1.5$ or 2.0, -3.5, and over 3.5.

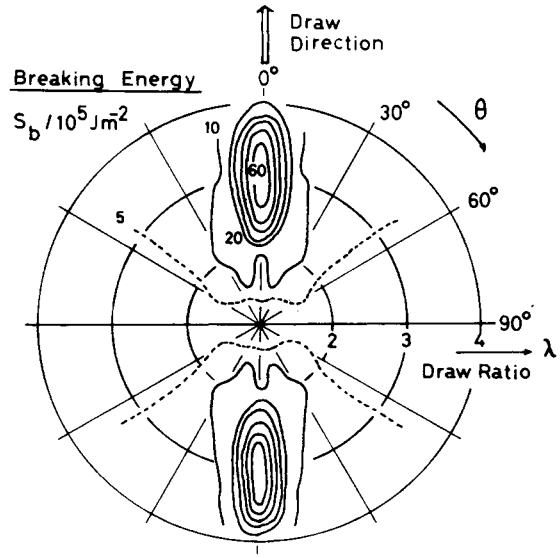

Fig. 7. Dependence of breaking energy S_b on draw ratio λ and cut-out angle θ for PET sheet at impacting speed of 10.5 m/sec = 1.8×10^4%/sec at 20° ± 1°C.

Orientational Behavior

The overall change in orientational behavior of macromolecular chains can be understood from the measurements of density and birefringence. Figure 8 shows the change in density with draw ratio. The density of PET sheet begins to increase from $\lambda = 1.75$; and especially at $\lambda > 2.0$–2.3, the increment becomes remarkable. The density decreases to some extent in the early stages of the orientation, up to $\lambda = 1.5$,[3,4] but this was not clear in the present study. The initial drawing temporarily gives rise to roughness in molecular packing (this may be related to the increase of free volume and mobility of molecular chains),[4] and further elongation gradually makes the polymer pack compactly. The orientational behavior obtained from the birefringence measurement is indicated by the orientation factor f_0 (Fig. 9). Generally, the orientation factor is defined as the quotient obtained by dividing the birefringence of the sample by that of a perfectly oriented one. Since birefringence is influenced by density, an appropriate correction is necessary, and f_0 is represented as follows[5,6]:

$$f_0 = (\Delta \cdot d_0)/(\Delta_0 \cdot d)$$

where Δ is the value for birefringence of the sample and d is its density, while Δ_0 and d_0 are the corresponding ideal values oriented perfectly along the stretching direction. The latter can be calculated from the crystal structure data. For PET, Δ_0 and d_0 are 216.5×10^{-3} and 1.455 g/cm^3, respectively.[7,8] The mean arrangement of molecular chains occurred in proportion to the elongation distance—even if there was nonhomogeneity in the structure of the starting material and the deformed places were different at each draw ratio.

From the microscopic view point, the chemical structure is associated with orientation behavior. The molecular chain of PET consists of rigid terephthalic acid and flexible ethylene glycol groups, which are not aligned in the same manner during the course of elongation. Conformational changes in PET have been interpreted using infrared and NMR data.[9–15] Recently, vibrational analysis was conducted by Boerio and Bahl.[16] Structural changes, due to various

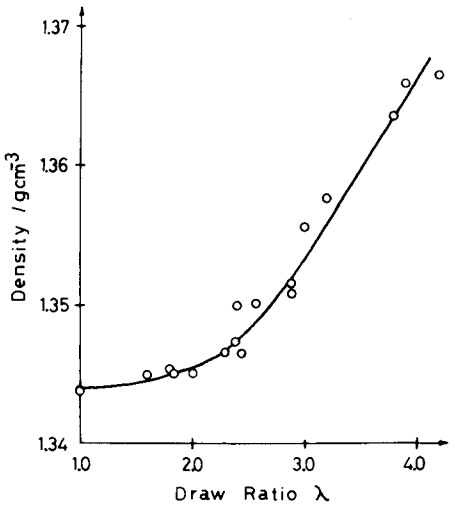

Fig. 8. Variation of density with draw ratio for PET sheet elongated at speed of 30%/min at 80°C.

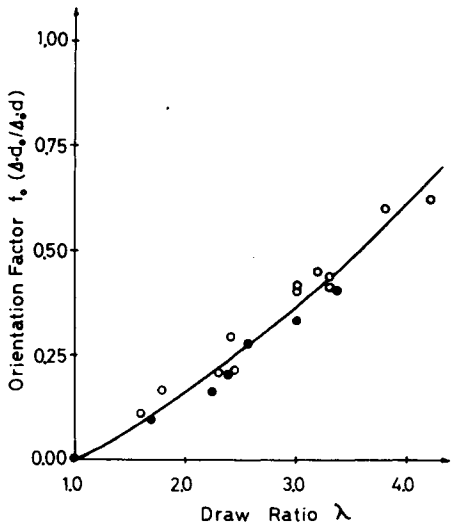

Fig. 9. Variation of orientation factor with draw ratio for PET sheet, calculated from the measurements of density d and birefringence Δ: (●) α-bromonaphthalene; (○) methylene diiodide.

treatments, are attributed to trans–gauche isomerism in the ethylene glycol segments of the molecules. Figure 10 shows the change of trans-form content with draw ratio,[17] using the 973 cm^{-1} band of the IR spectrum (assigned to the C—O stretching mode). In the early stage of orientation the content of the trans form decreases slightly, in a similar manner to the change in density,[3,4] and then increases with further elongation. By assigning IR absorption bands and classifying those where there is an increase or decrease in dichroism with draw ratio, Ito, however, found that the orientation of the terephthalic acid segments dominates over that of the ethylene glycol segments.[18] According to the magnetic anisotropy measurements, a linear relationship existed between anisotropy and draw ratio (consisting of two sections) and the critical point located at λ = 3.8.[9] From the above experimental facts, the orientational behavior in molecular dimension may be grouped into three steps of draw ratio: $\lambda = -1.5$ or 2.0, − 3.5,

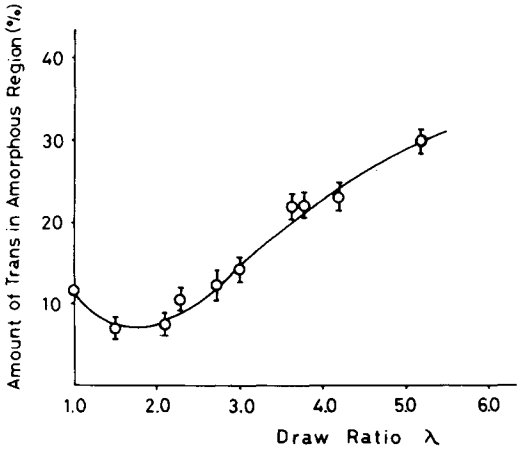

Fig. 10. Change of trans form content of C—O bond of the ethylene glycol segment of PET with draw ratio.

and over 3.5. This classification agrees with the results from tensile impact testing. Impact characteristics reflect the structural anisotropy and the orientation state of the polymer.

Fracture Morphology

The amorphous quench-rolled PET (starting material) is in the nonhomogeneous state, and the structural change due to stretching appears on the breaking surfaces of the specimens. A series of the breaking surfaces are shown in Figure 11 (magnification ×1000). The starting material consists of masses with the dimensions of 20–30 μm, the boundary of which is not clear until adiabatic deformation (mechanical impact) is applied. During low draw ratio, deformation occurs at the boundaries of the masses which become fibril-like, Figure 11(a). Simultaneously, the masses become distorted along the stretching direction. Since the deformation rate is different between the masses and their boundaries, a part with relatively low density should occur in the early stage of elongation. When new voids have not occurred, this part must supplement its expansion by its own molecular volume through segmental motion. This may be correlated with the relative increase of the gauche form of the ethylene glycol segments (Fig. 10). Passing through a certain limit of deformation (λ = ca. 2.0 in PET), the specimens begin to show ductility. Although the details were not known because of plastic deformation, traces of the deformed masses are observed, Figure 11(c). At $\lambda > 3.5$, where brittle-like fracture occurs again, the breaking surfaces were relatively simple, Figures 11(d) and (e). This may be due to partial quasi-melting by the abrupt elevation of temperature due to adiabatic deformation. Therefore, information regarding the structure was not clear.

CONCLUSION

Tensile impact testing results indicated the occurrence of structural anisotropy by stretching of isotropic amorphous quench-rolled PET. This is related to the deformation mechanisms of masses with dimensions a few tenths of a μm and their boundaries. The presence of maximum E and σ_m in the direction of θ = 30° during low draw ratio may also be correlated to the above deformation mechanism, but details cannot be interpreted at the present time. For $\lambda > 2.0$, the masses become increasingly distorted, and the structures of the deformed masses themselves are reflected in the mechanical properties. Although the orientation factor increases (Fig. 9), the quantity of the trans form is relatively minor (Fig. 10), and the observed Young's modulus is considerably smaller (for example, $E = 16 \times 10^9$ N/m^2 at $\lambda = 4.02$), compared with the theoretical E = 95–122 $\times 10^9$ N/m^2.[19,20] Moreover, the mechanical properties do not change for the range of cut-out angle θ = 45–90°. This means that the area supporting the mechanical strength is limited to one small section, and its characteristics are not affected by macroscopic deformation except in the direction parallel to or near the stretching direction. To obtain further information, it would be necessary to consider the structure of the deformed masses in the superstructure.

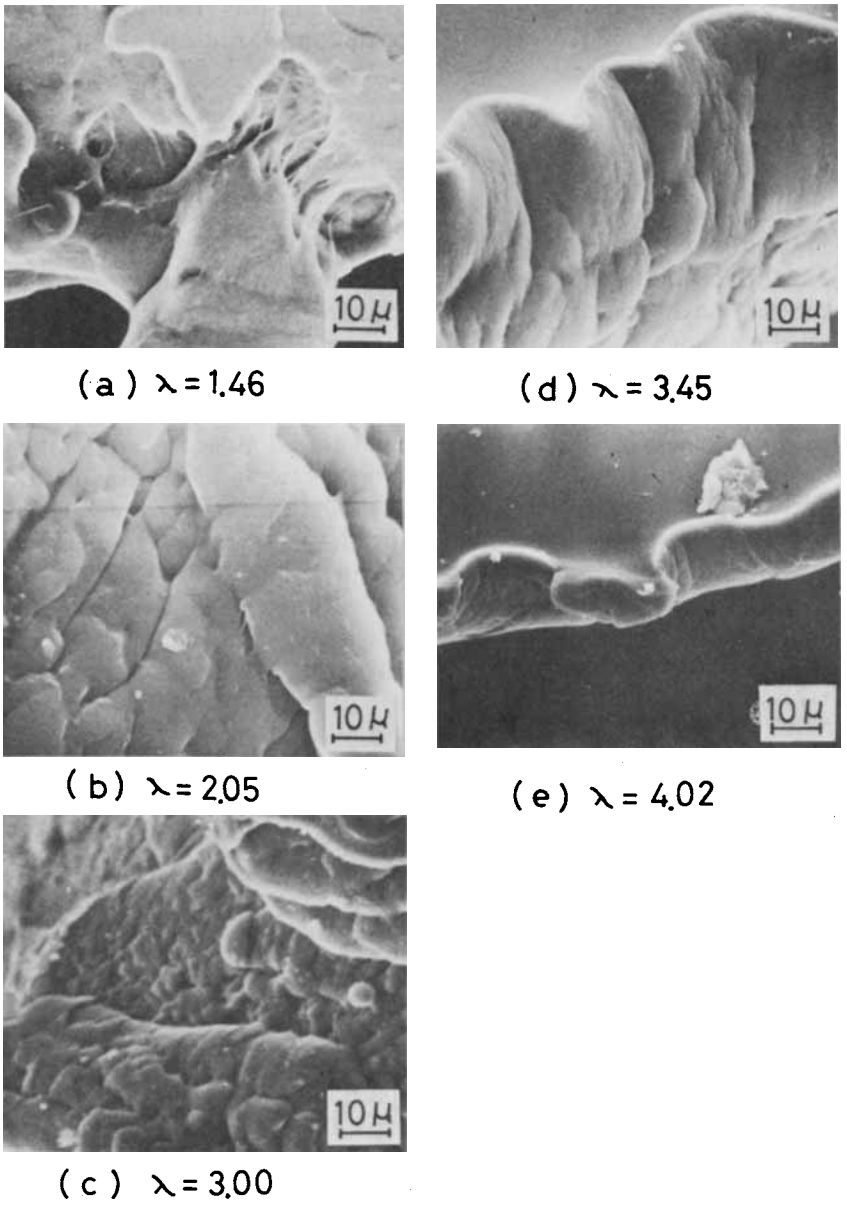

Fig. 11. Photographs of breaking surfaces of PET sheet (drawn at speed of 30%/min at 80°C) after tensile impact testing at speed of 10.5 m/sec = 1.8×10^4%/sec at 20° ± 1°C. The draw ratio λ was changed, and the cut-out angle θ was constant (parallel to the stretching direction), ×1000.

The authors thank Dr. Mitsuishi of Teijin Co. Ltd. for his generous supply of amorphous quench-rolled PET sheets.

References

1. M. Yokouchi and Y. Kobayashi, *J. Appl. Polym. Sci.*, **24,** 29 (1979).
2. M. Yokouchi and Y. Kobayashi, *Rep. Asahi Glass Fund. Ind. Tech.*, **33,** 241 (1978).
3. E. Ito, S. Okajima, H. Sasabe, and S. Saito, *Kolloid-Z. Z. Polym.*, **251,** 579 (1973).

4. D. F. Kagen, R. M. Tyulina, S. V. Vlasov, and L. D. Samarina, *Vysokomol. Soedin.*, **A19,** 712 (1977).
5. P. H. Hermans, *Contribution to the Physics of Cellulose Fibres,* Elsvier, Amsterdam, 1946.
6. Y. Kobayashi, *Sen-i to Kogyo,* **3,** 665 (1970).
7. M. Kuriyama, K. Tomishima, and K. Shirakashi, *Sen-i Gakkaishi,* **20,** 431 (1964).
8. R. P. de Daubeny, C. W. Bunn, and C. J. Brown, *Proc. Roy. Soc.,* **A226,** 531 (1954).
9. P. W. Selwood, J. A. Parodi, and A. Pace, Jr., *J. Am. Chem. Soc.,* **72,** 1269 (1950).
10. W. W. Daniels and R. E. Kitson, *J. Polym. Sci.,* **33,** 161 (1958).
11. A. Miyake, *J. Polym. Sci.,* **38,** 479 (1959).
12. G. Farrow, J. McIntosh, and I. M. Ward, *Macromol. Chem.,* **38,** 147 (1960).
13. I. M. Ward, *Text. Res. J.,* **31,** 650 (1961).
14. P. G. Schmidt, *J. Polym. Sci., Part A-1,* **1,** 1271 (1963).
15. J. L. Koenig and S. W. Cornell, *J. Polym. Sci., Part C,* **22,** 1019 (1969).
16. F. J. Boerio and S. K. Bahl, *J. Polym. Sci., Polym. Phys. Ed.,* **14,** 1029 (1976).
17. T. Hogi, Y. Kobayashi, and S. Okajima, unpublished results.
18. E. Ito, *Dissertation,* Tokyo Metropolitan University, 1971.
19. K. Tashiro, M. Kobayashi, and H. Tadokoro, *Macromolecules,* **10,** 413 (1977).
20. L. R. G. Treloar, *Polymer,* 1, 95, 279, 290 (1960).

Received November 15, 1978
Revised June 22, 1979